

DFTT 34/94
August 1994

SIGNALS OF NEUTRALINO DARK MATTER FROM EARTH AND SUN

A. BOTTINO, N. FORNENGO, G. MIGNOLA

*Dipartimento di Fisica Teorica, Università di Torino and
INFN, Sezione di Torino, via P.Giuria 1, 10125 Torino, Italy*

and

L. MOSCOSO

*DAPNIA/DSM/SPP
CE-Saclay, 91191 Gif-sur-Yvette, France*

Abstract

We evaluate the fluxes of up-going muons detectable in a neutrino telescope and due to the annihilation of relic neutralinos in the Earth and in the Sun, taking realistically into account the fact that neutralinos might provide only a fraction of the local (solar neighbourhood) dark matter (DM). We determine the relation between the exposure At of the neutrino telescope (A being the telescope area, t the live time) and the explorable range of the neutralino mass and composition, when the signal-to-background ratio is optimized by an appropriate angular selection.

(to appear in *Astroparticle Physics*)

E-mail addresses: (bottino, fornengo, mignola)@to.infn.it
moscoso@saclay.cea.fr

1 Introduction

The perspectives of observing, with neutrino telescopes of large area, indirect signals of relic neutralinos from celestial bodies (Earth and Sun) are very appealing and are currently the subject of much investigation [1–3]. The sequence of the physical processes which could produce these signals are: i) capture of relic neutralinos by the macroscopic bodies; ii) subsequent accumulation of these particles in a region around the centre of these celestial objects; iii) pair annihilation of the accumulated neutralinos which would generate, by decay of the particles produced in the various annihilation final states, an output of high-energy neutrinos. These neutrinos may be detected in a neutrino telescope in two ways: either by looking at events due to the ν -interactions inside the detector (contained events) or by measuring the muons which are produced by ν_μ and $\bar{\nu}_\mu$ interactions in the rock around the detector and then traverse it upwardly. In the present paper we only discuss the latter case; we address the problem of the theoretical predictions for the fluxes of these up-going muons in a neutrino telescope and of their discrimination against the background due to atmospheric neutrinos. The present analysis aims at improving the previous ones in many instances: a) The calculations of the predicted signals for both macroscopic bodies (Earth and Sun) are presented in a common theoretical framework; in particular, this enables a comparative discussion about the informations obtainable by measurements of the two fluxes. b) It is realistically taken into account the fact that neutralinos might provide only a fraction of the local (solar neighbourhood) dark matter (DM) density. In order to establish whether and by how much the total DM density has to be rescaled, the neutralino relic abundance is explicitly evaluated at any point of the model parameter space where signals are calculated. c) It is finally discussed the relation between the exposure At of a neutrino telescope (A being the telescope area, t the live time) and the explorable range of the neutralino mass (and composition), taking into account the optimization of the signal-to-background ratio (S/B).

The theoretical framework adopted in the present paper is the one provided by the Minimal Supersymmetric extension of the Standard Model (MSSM) [4], which, implemented by a general grand unification relation, may be formulated (for the neutralino sector) in terms of only three parameters: two mass parameters M_2 and μ , and a third parameter $\tan\beta$ defined as $\tan\beta = v_u/v_d$ (v_u and v_d are the v.e.v.'s that give masses to the up-type and down-type quarks, respectively). The neutralino, χ , is defined to be the lowest-mass linear combination of the two gauginos (photino and zino) and the two higgsinos

$$\chi = a_1\tilde{\gamma} + a_2\tilde{Z} + a_3\tilde{H}_1^0 + a_4\tilde{H}_2^0. \quad (1)$$

Here $\tilde{\gamma}$ and \tilde{Z} are the fields obtained from the original fields for the U(1) and SU(2) neutral gauginos, \tilde{B} and \tilde{W}_3 , by a rotation in terms of the Weinberg angle.

It is useful to introduce a composition parameter $P = a_1^2 + a_2^2$ which gives the gaugino fractional weight. The neutralino mass m_χ and the coefficients a_i 's depend on the three model parameters M_2 , μ and $\tan\beta$. Since almost everywhere in the parameter space

there is a one-to-one correspondence: $(M_2, \mu) \leftrightarrow (P, m_\chi)$, at fixed $\tan \beta$, in the following we will use as a set of independent parameters: P , m_χ and $\tan \beta$. This allows us to present our results in terms of two quantities, P and m_χ , which have a direct physical meaning for the neutralino. In the following, for $\tan \beta$, unless differently specified, we will use the representative value $\tan \beta = 8$.

We still have to state which values we assign to the unknown masses of the Higgs bosons and of the sfermions; in fact these masses enter in the theoretical calculations, since Higgses and sfermions play a crucial role in the physical processes initiated by neutralinos. As for the neutral Higgs bosons, we recall that in the MSSM there are three neutral Higgs particles: two CP-even bosons h and H (of masses m_h , m_H with $m_H > m_h$) and a CP-odd one A (of mass m_A). Once a value for one of these masses (say, m_h) is assigned, the other two masses (m_A , m_H) are derived through mass relationships depending on radiative effects. In the present paper the Higgs mass m_h is set at the value of 50 GeV. As for the sfermion masses, these are set here at the value $m_{\tilde{f}} = 1.2 m_\chi$, when $m_\chi > 45$ GeV, $m_{\tilde{f}} = 45$ GeV otherwise. Only the mass of the stop quark is assigned a larger value of 1 TeV. The top mass is fixed at $m_t = 170$ GeV.

2 Neutralino local density

An important quantity that enters in the capture rate of relic neutralinos by macroscopic bodies is the neutralino local density ρ_χ . One can assume that ρ_χ is equal to the local value of the total DM density ρ_l , when the neutralino relic abundance ($\Omega_\chi h^2$) turns out to be at the level of an $(\Omega h^2)_{\min}$ consistent with ρ_l . On the contrary when $(\Omega_\chi h^2)$ is smaller than $(\Omega h^2)_{\min}$ the value to be assigned to ρ_χ has to be appropriately reduced. Thus we evaluate $\Omega_\chi h^2$ and we determine ρ_χ by adopting a standard rescaling procedure [5]:

$$\begin{aligned} \rho_\chi &= \rho_l, & \text{when } \Omega_\chi h^2 &\geq (\Omega h^2)_{\min} \\ \rho_\chi &= \rho_l \frac{\Omega_\chi h^2}{(\Omega h^2)_{\min}}, & \text{when } \Omega_\chi h^2 < (\Omega h^2)_{\min} \end{aligned} \quad (2)$$

Here $(\Omega h^2)_{\min}$ is set equal to 0.03. For ρ_l , we have used the value $\rho_l = 0.3 \text{ GeV cm}^{-3}$.

The neutralino relic abundance $\Omega_\chi h^2$ is evaluated here following the procedure illustrated in Ref. [6]. By way of example in Fig.1 we display $\Omega_\chi h^2$ as a function of m_χ for three representative neutralino compositions: i) a gaugino-dominated composition ($P = 0.9$), ii) a composition of maximal gaugino-higgsino mixing ($P = 0.5$), iii) a higgsino-dominated composition ($P = 0.1$). As expected, out of the three compositions displayed in Fig.1, the gaugino-dominated state provides the largest values of $\Omega_\chi h^2$. More substantial values of $\Omega_\chi h^2$ occurs if one considers purer gaugino compositions ($P \gtrsim 0.99$), as shown in Fig.2, where, together with the reference value $P = 0.5$, are also displayed the rather extreme cases: $P = 0.01$ (very pure higgsino composition) and $P = 0.99$ (very pure gaugino composition). The very pronounced dips in the plots of Figs 1–2 are due to the s-poles in the χ - χ annihilation cross section (exchange of the Z and of the neutral Higgs bosons).

Displayed in Fig.3 are the values of $\Omega_\chi h^2$ versus m_χ in the form of scatter plots obtained by varying M_2 and μ over a grid of constant spacing in a log-log plane over the ranges $20 \text{ GeV} \leq M_2 \leq 6 \text{ TeV}$, $20 \text{ GeV} \leq |\mu| \leq 3 \text{ TeV}$. By comparing Fig.3 with Fig.2 one sees that the large spread in values for $\Omega_\chi h^2$, displayed in Fig.3, is due to configurations of extremely pure composition.

3 Capture rates and annihilation rates

The capture rate C of the relic neutralinos by a macroscopic body may be evaluated by the standard formula [7]

$$C = \frac{\rho_\chi}{v_\chi} \sum_i \frac{\sigma_{\text{el},i}}{m_\chi m_i} (M_B f_i) \langle v_{\text{esc}}^2 \rangle_i X_i, \quad (3)$$

where v_χ is the neutralino mean velocity, $\sigma_{\text{el},i}$ is the cross section of the neutralino elastic scattering off the nucleus i of mass m_i , $M_B f_i$ is the total mass of the element i in the body of mass M_B , $\langle v_{\text{esc}}^2 \rangle_i$ is the square escape velocity averaged over the distribution of the element i , X_i is a factor which takes account of kinematical properties occurring in the neutralino-nucleus interactions. The elastic χ -nucleus cross sections are evaluated according to the method presented in Ref. [8].

The annihilation rate Γ_A is expressed in terms of the capture rate by the formula [9]

$$\Gamma_A = \frac{C}{2} \tanh^2\left(\frac{t}{\tau_A}\right) \quad (4)$$

where t is the age of the macroscopic body ($t = 4.5 \text{ Gyr}$ for Sun and Earth), $\tau_A = (CC_A)^{-1/2}$, and C_A is the annihilation rate per effective volume of the body, given by

$$C_A = \frac{\langle \sigma v \rangle}{V_0} \left(\frac{m_\chi}{20 \text{ GeV}} \right)^{3/2} \quad (5)$$

V_0 is defined as $V_0 = (3m_{Pl}^2 T / (2\rho \times 10 \text{ GeV}))^{3/2}$ where T and ρ are the central temperature and the central density of the celestial body. For the Earth ($T = 6000 \text{ K}$, $\rho = 13 \text{ g} \cdot \text{cm}^{-3}$) $V_0 = 2.3 \times 10^{25} \text{ cm}^3$, for the Sun ($T = 1.4 \times 10^7 \text{ K}$, $\rho = 150 \text{ g} \cdot \text{cm}^{-3}$) $V_0 = 6.6 \times 10^{28} \text{ cm}^3$. σ is the neutralino-neutralino annihilation cross section and v is the relative velocity. $\langle \sigma v \rangle$ is calculated with all the contributions at the tree level as in Ref.[6], with the further inclusion here of the two gluon annihilation final state [10].

We recall that, according to Eq.(4), in a given macroscopic body the equilibrium between capture and annihilation (*i.e.* $\Gamma_A \sim C/2$) is established only when $t \gtrsim \tau_A$. It is worth noticing that the neutralino density ρ_χ , evaluated according to Eq.(2), enters not only in C but also in τ_A (through C). Therefore the use of a correct value for ρ_χ (rescaled according to Eq.(2), when necessary) is important also in determining whether or not the equilibrium is already set in a macroscopic body.

In Fig.4 we give the results of our calculations for $\tanh^2(t/\tau_A)$ and for Γ_A in the case of the Earth for three representative χ -compositions: $P = 0.1, 0.5, 0.9$. For simplicity, in these figures, as well as in the following ones, only the results concerning positive values of the parameter μ are shown; similar results hold for negative values of μ . The upper part of Fig.4 shows that the equilibrium between capture and annihilation is not reached for $m_\chi \gtrsim m_W$; thus a substantial suppression occurs in Γ_A at large values of m_χ because of the factor $\tanh^2(t/\tau_A)$. In Fig.5 the two quantities $\tanh^2(t/\tau_A)$ and Γ_A are plotted for other representative values of neutralino compositions: $P = 0.01, 0.99$ (the value $P = 0.5$ is shown again for comparison). In Figs 4–5 we see that, for $m_\chi \lesssim 70$ GeV, Γ_A shows the characteristic bumps due to fact that the capture is very efficient when the neutralino mass matches the nuclear mass of some important chemical component of the Earth (O, Si, Mg, Fe). Superimposed to these properties are the features due to the rescaling of ρ_χ . In fact this rescaling implies here both a general suppression and the appearance of the peculiar dips reminiscent of the singularities in the annihilation cross section (discussed in Sect. 2). For comparison with Fig.4 we show in Fig.6 how the two quantities $\tanh^2(t/\tau_A)$ and Γ_A would appear, if the rescaling were not applied.

Whereas for the Earth the equilibrium condition depends sensitively on the values of the model parameters, in the case of the Sun equilibrium between capture and annihilation is reached for the whole range of m_χ , due to the much more efficient capture rate implied by the stronger gravitational field [7]. Γ_A for the Sun is shown in Fig.7.

What we have defined above is the annihilation rate referred to a macroscopic body as a whole. This is certainly enough for the Sun which appears to us as a point source. On the contrary, in the case of the Earth, one has also to define an annihilation rate referred to a unit volume at point \vec{r} from the Earth center

$$\Gamma_A(r) = \frac{1}{2} \langle \sigma v \rangle n^2(r) \quad (6)$$

where $n(r)$ is the neutralino spatial density which may be written as [9]

$$n(r) = n_0 e^{-\alpha m_\chi r^2}; \quad (7)$$

here $\alpha = 2\pi G\rho/(3T)$ and n_0 is such that

$$\Gamma_A = \frac{1}{2} \langle \sigma v \rangle \int d^3r n^2(r). \quad (8)$$

4 Neutrino fluxes

The differential neutrino flux due to χ - χ annihilation in a distant source (Sun) is given by

$$\frac{dN_\nu}{dE_\nu} = \frac{\Gamma_A}{4\pi d^2} \sum_{F,f} B_{\chi f}^{(F)} \frac{dN_{f\nu}}{dE_\nu} \quad (9)$$

where d is the distance from the source, F denotes the χ - χ annihilation final states, $B_{\chi f}^{(F)}$ denotes the branching ratios into heavy quarks, τ lepton and gluons in the channel F ; $dN_{f\nu}/dE_\nu$ is the differential distribution of the neutrinos generated by the hadronization of quarks and gluons and the subsequent hadronic semileptonic decays.

In the case of the Earth we define a differential neutrino flux generated at a distance R by the χ - χ annihilations which take place at a point \vec{r} from the center of the Earth

$$\frac{dN_\nu}{dE_\nu d^3r} = \frac{\langle \sigma v \rangle n^2(r)}{8\pi R^2} \sum_{F,f} B_{\chi f}^{(F)} \frac{dN_{f\nu}}{dE_\nu} \quad (10)$$

This is the neutrino spectrum which is used in our Monte Carlo code to evaluate the flux of up-going muons, as illustrated in Sect. 5.

However, it is also useful to write the neutrino differential flux at a point on the Earth surface, once the integration over the distribution $n(r)$ is performed, at fixed nadir angle θ [7]

$$\frac{d^2N_\nu}{dE_\nu d\cos\theta} = G(\theta) \frac{\Gamma_A}{4\pi R_\oplus^2} \sum_{F,f} B_{\chi f}^{(F)} \frac{dN_{f\nu}}{dE_\nu}. \quad (11)$$

$G(\theta)$ is given by

$$G(\theta) \simeq 2(2m\beta)e^{-2m\beta \sin^2 \theta} \quad (12)$$

where $\beta = \alpha R_\oplus^2$, for $m_\chi \gtrsim 10$ GeV and $\theta \lesssim 60^\circ$. This flux, as all other fluxes discussed afterwards, refer to surfaces orthogonal to the incoming direction.

As far as the differential neutrino spectra are concerned, we briefly quote the relevant ingredients that we used in the calculation. A Jetset 7.2 Monte Carlo [11] code was used to compute the neutrino spectra due to b and c quarks, tau lepton and gluons. Following Ref. [12] we have neglected the contributions of the light quarks directly produced in the annihilation process or in the hadronization of heavy quarks and gluons, because these light particles stop inside the medium (Sun or Earth) before their decay. For the case of the Sun also the energy loss of the heavy hadrons in the solar medium was considered. The spectra due to heavier final states, *i.e.* Higgs bosons, gauge bosons and t quark, were computed analytically by following the decay chain down to the production of a b quark, c quark or a tau lepton; the result of the Monte Carlo was used to obtain the final neutrino

output. Because of the high column density of the solar medium, the absorption and the energy loss of the produced neutrinos were also included.

As an example, we show in Fig.8 the neutrino spectra for neutralino annihilation in the Earth, for $P = 0.5$ and for three different values of the neutralino mass: $m_\chi = 20, 40$ and 120 GeV. The different shapes depend on which final states dominate in the annihilation cross section. For instance the spectrum at $m_\chi = 120$ GeV shows the typical features due to the opening of the W^+W^- final state in the $\chi\chi$ annihilation. The relative magnitudes of the spectra at different values of m_χ are driven by the dependence of the annihilation rate Γ_A on the model parameters.

5 Signals of up-going muons

Let us turn now to the calculation of the various distributions and rates for the up-going muons generated by the neutrino fluxes of Eq.s(9–10) (signals) and by the neutrinos produced in the Earth atmosphere (background). The conversion of the muon neutrinos into muons and the subsequent muon propagation up to the detector have been treated using a Monte Carlo simulation.

The muon flux at the detector depends on the following quantities: the neutrino energy spectrum and spatial distribution, the differential $\nu_\mu - N$ charged current cross section for the muon production and the energy losses and the multiple scattering of the muon in the rock surrounding the detector.

As for the signals, the neutrino energies have been generated in the range $2 \text{ GeV} \leq E_\nu \leq m_\chi$ according to the distributions of Eq.(9) for the Sun and of Eq.(10) for the Earth. We emphasize that in the latter case the neutrino production point has been generated in a region around the Earth center with a gaussian distribution $n^2(r)$, where $n(r)$ is given in Eq.(7). The atmospheric neutrinos have been generated upwardly according to the differential distribution given by [13] for neutrinos with $E_\nu \leq 100 \text{ GeV}$ and by [14] for neutrinos with $E_\nu > 100 \text{ GeV}$.

In the cross section for the charged current $\nu_\mu - N$ deep inelastic scattering we have employed the CTEQ parton distribution functions [15]. The energy losses and multiple scattering of the muon have been calculated by propagating the muon in standard rock by steps of 10^4 g cm^{-2} when the muon energy was larger than 30 GeV , of 500 g cm^{-2} when it was between 1.2 and 30 GeV , and equal to $E_\mu / (2.4 \cdot 10^{-3} \text{ GeV}) \text{ g cm}^{-2}$ for the final step when $E_\mu < 1.2 \text{ GeV}$. The residual energy and the muon direction were kept in memory for each step from the muon production to the muon stopping. The detector entry point has been randomly generated with a uniform probability along the whole muon track. The muon energy and direction at the entry point has been calculated by interpolating between the initial and final values for the step where the entry point occurred. A random angle has been included to take into account a detector angular resolution of 2° .

6 Results and conclusions

We show in Figs 9–11 a sample of our results for the signals expected from the Earth at the usual representative point $\tan \beta = 8$ (for the fluxes and the angular distributions shown in these figures and in the following ones the threshold for the muon energy is set at the value $E_\mu^{\text{th}} = 2$ GeV). Fig.9 displays the integral muon flux versus m_χ for various neutralino compositions. This has been obtained with a no-straggling approximation [16], *i.e.* the muons are produced and propagated in the forward direction (when this approximation is applied, then Eq.(11) for the neutrino distribution is useful). The general structure of the flux clearly reflects the features of the annihilation rate in Earth, previously discussed. The horizontal line represents the Kamiokande upper bound for signals coming from the Earth [2]: $4.0 \cdot 10^{-14} \text{cm}^{-2} \text{s}^{-1}$ (90 % C.L.); this value refers to a half-aperture of $\theta_t = 30^\circ$ for a cone centered at the nadir. By comparing this upper limit with our fluxes we see that the regions explored by Kamiokande (at our representative point: $\tan \beta = 8, m_h$ and $m_{\tilde{f}}$ chosen as stated in Sect. 1) concern the neutralino mass range $50 \text{ GeV} \lesssim m_\chi \lesssim 80 \text{ GeV}$, for $0.1 \lesssim P \lesssim 0.9$; the mass range is narrower for purer neutralino compositions.

By way of example we show in Figs 10–11 the differential spectra and the angular distributions for the case $P = 0.5$ and $m_\chi = 120 \text{ GeV}$. In Fig.10 the spectra obtained with the MC code for the expected signal and for the background are displayed by the two histograms. The solid line represents the spectrum for the signal obtained with the no-straggling approximation; it is clear from the plot that this approximation is quite good for the spectrum, and then also for the integrated flux. The spectra shown in this figure refer to the muons entering the detector within a cone of half-aperture $\theta_t = 30^\circ$ centered at the nadir. In Fig.11 the angular distribution due to the signal, markedly peaked around the nadir direction, is compared with the almost flat background distribution.

Now a very relevant question is what is the minimal exposure At necessary to provide a good S/B discrimination. To put it into a more quantitative way, we define an $(At)_{\text{min}}$ as the minimal exposure necessary to see a 4σ effect (with a signal of at least 4 events) [17]. $(At)_{\text{min}}$ is displayed in Fig.12a (the angle θ_t of half-aperture from the nadir is again set at the value $\theta_t = 30^\circ$ here). However, it is important to remark that, due to the different features of the angular distributions for the signal and for the background (illustrated for instance in Fig.11), $(At)_{\text{min}}$ may be optimized by appropriately choosing the angular window, *i.e.* θ_t . We call $(At)_{\text{opt}}$ the least value of $(At)_{\text{min}}$ when θ_t is varied, and we denote by θ_{opt} the corresponding value of θ_t . This optimization procedure has to be applied to $(At)_{\text{min}}$ for each value of the integral flux Φ_μ . For the case illustrated in Fig.11 we find $\theta_{\text{opt}} \simeq 5^\circ$, $(At)_{\text{opt}} \simeq 3020 \text{ m}^2 \text{ yr}$. Fig.12b displays the dependence of $(At)_{\text{opt}}$ on m_χ and P for our usual representative case. To obtain the result of Fig.12b the optimization, based on the angular distribution, has been performed by using the results of the MC simulations at 4 values of the neutralino mass: $m_\chi = 20, 40, 60, 120 \text{ GeV}$, by interpolating between these values and by conservatively using for $m_\chi > 120 \text{ GeV}$ the same angular window as for $m_\chi = 120 \text{ GeV}$. For the integral flux we employed the results (shown in Fig.9a) obtained with the no-straggling approximation. By comparing Figs 12a and 12b one sees that the optimization improves significantly the experimental capabilities especially at large m_χ values; in fact for these values the extension of the annihilation region is very

much concentrated around the Earth center. Fig.12b shows realistically by which amount the explorable ranges of the two neutralino parameters m_χ and P increase as the exposure At is increased. We remind that the largest value for At obtained up to now is the one of Kamioka: $At = 770 \text{ m}^2 \text{ yr}$ [2]. A sizeable improvement in At will be provided by MACRO [18].

Let us turn now to the signals from the Sun. In Fig.13 the relevant flux of up-going muons is plotted versus m_χ in the case of the representative point under discussion; Φ_μ is the flux through a surface orthogonal to the Sun direction. The horizontal line denotes the present upper bound of $6.6 \cdot 10^{-14} \text{ cm}^{-2} \text{ s}^{-1}$ (90 % C.L.) (an half-aperture $\theta = 25^\circ$ was taken here for a cone centered at the Sun direction) [2]. It is clear that this limit does not introduce any constraint here. In Fig.14 the corresponding $(\epsilon At) - m_\chi$ plot is displayed (a cone of 5° half-aperture around the Sun direction has been used for the evaluation of the background, ϵ is the on-source duty factor). In this plot we see that, in order to start some exploration about relic neutralinos using the flux from the Sun, one needs at least $(\epsilon At) \simeq 10^4 \text{ m}^2 \text{ yr}$ (this could provide information in the range $70 \text{ GeV} \lesssim m_\chi \lesssim 150 \text{ GeV}$). However, it is remarkable that by slightly increasing (ϵAt) above this level, the explorable range in terms of P and m_χ expands quite rapidly towards the high values of the neutralino mass.

An interesting point concerns the relative importance of the up-going muon fluxes from the Earth and from the Sun. As we see from Figs (9,13), for light neutralinos the signal from the Sun is much smaller than the signal from the Earth; as m_χ increases the signal from the Sun may overcome the other, since the Sun gravitational field is much more efficient in capturing the neutralinos. More relevant for a comparative discussion about the signals from the two sources are the two diagrams of the exposure versus m_χ displayed in Figs 12b, 14. A very appealing situation is the one where the signals from both sources could be detected. For instance, assuming $\epsilon \simeq 0.5$, an exposure $At \simeq 10^5 \text{ m}^2 \text{ yr}$ would be sensitive to both signals in the range $35 \text{ GeV} \lesssim m_\chi \lesssim 200 \text{ GeV}$.

A word of warning is in order here to remind that the present evaluations depend sensitively on a number of free parameters. As far as $\tan\beta$ is concerned, we may notice that the dependence of the signals on this parameter is rather involved, but, as a general trend, the expected signals increase with the value of $\tan\beta$. For instance, for the Sun, moving from the value $\tan\beta = 8$ to the value $\tan\beta = 20$ the flux is enhanced by about a factor 5 for $m_\chi \gtrsim 200 \text{ GeV}$; but, if the value of $\tan\beta$ is reduced from $\tan\beta = 8$ to $\tan\beta = 2$, the flux is suppressed (for $m_\chi \gtrsim 50 \text{ GeV}$) roughly by an order of magnitude. The quantities calculated in the present paper are also rather sensitive on the values employed for the Higgs and the sfermion masses. For instance, our signals for the Earth are roughly proportional to m_h^{-4} . In the present paper we have used for the Higgs and the sfermion masses values close to their present lower bounds. This choice enables one to establish, by use of the figures previously reported, what is the minimum exposure necessary for a detector to be sensitive to the Earth and/or Sun signals and how the exploration into the DM neutralino properties may be progressively improved by expanding the size of the experimental apparatus.

To summarize we may conclude that the exploration in the realm of the relic neutralinos by neutrino telescopes, after the first insights provided by Kamiokande [2] about the Earth signals, will certainly be significantly developed by the underwater (under-ice) detectors under construction [3]. In order to have good perspectives for a systematic investigation of this field one should finally aim at an apparatus of very large area of order of 10^6 m^2 .

Acknowledgments

We are grateful to professor V. S. Berezinsky for very interesting discussions.

References

- [1] G.F. Giudice and E. Roulet, *Nucl. Phys.* **B316** (1989) 429;
 G.B. Gelmini, P. Gondolo and E. Roulet, *Nucl. Phys.* **B351** (1991) 623;
 M. Kamionkowski, *Phys. Rev.* **D44** (1991) 3021;
 A. Bottino, V. de Alfaro, N. Fornengo, G. Mignola and M. Pignone, *Phys. Lett.* **B265** (1991) 57;
 F. Halzen, M. Kamionkowski and T. Steltzer, *Phys. Rev.* **D45** (1992) 4439;
 V.S. Berezinsky, *Nucl. Phys.* (Proc. Suppl.) **B31** (1993) 413 (Proc. Neutrino 92, Ed. A. Morales)
 M. Mori et al., *Phys. Rev.* **D48** (1993) 5505;
 M. Drees, G. Jungman, M. Kamionkowski and M.M. Nojiri, *Phys. Rev.* **D49** (1994) 636;
 R. Gandhi, J.L. Lopez, D.V. Nanopoulos, K. Yuan and A. Zichichi, *Phys. Rev.* **D49** (1994) 3691.
- [2] M. Mori et al. (Kamiokande Collaboration), *Phys. Lett.* **B289** (1992) 463.
- [3] J.G. Learned, *Nucl. Phys.* (Proc. Suppl.) **B31** (1993) 456 (Proc. Neutrino 92, Ed. A. Morales);
 F. Halzen, *Proc. Fourth International Workshop on Neutrino Telescopes* (1992), Ed. M. Baldo Ceolin;
 G.V. Domogatsky, *Nucl. Phys.* (Proc. Suppl.) **B35** (1994) 290 (Proc. TAUP 93, Ed.s C.Arpesella, E.Bellotti, A.Bottino);
 L.K. Resvanis, *loc. cit.* 294.
- [4] H.P. Nilles, *Phys. Rep.* **110** (1984) 1;
 H.E. Haber and G.L. Kane, *Phys. Rep.* **117** (1985) 75;
 R. Barbieri, *Rivista Nuovo Cimento* **11** (1988) 1.
- [5] T.K. Gaisser, G. Steigman and S. Tilav, *Phys. Rev.* **D34**(1986)2206.
- [6] A. Bottino, V.de Alfaro, N. Fornengo, G. Mignola and M. Pignone, *Astroparticle Physics* **2** (1994) 67.
- [7] A. Gould, *Ap. J.* **321** (1987) 571; *Ap. J.* **328** (1988) 919; *Ap. J.* **368** (1991) 610.
- [8] A. Bottino, V. de Alfaro, N. Fornengo, A. Morales, J. Puimedón and S. Scopel, *Mod. Phys. Lett.* **A7** (1992) 733. Notice that in the present paper for the Higgs boson–nucleon coupling we use the evaluation of J. Gasser, H. Leutwyler and M. E. Sainio, *Phys. Lett.* **B253** (1991) 252.
- [9] K. Griest and D. Seckel, *Nucl. Phys.* **B283** (1987) 681.
- [10] M. Drees, G. Jungman, M. Kamionkowski and M.M. Nojiri, *Phys. Rev.* **D49** (1994) 636.

- [11] T. Sjöstrand, *Comp. Phys. Comm.* **39** (1986) 347; *Comp. Phys. Comm.* **43** (1987) 367; CERN-TH 6488/92.
- [12] S.Ritz and D.Seckel, *Nucl. Phys.* **B304** (1988) 877.
- [13] G. Barr, T.K. Gaisser and T. Stanev, *Phys. Rev.* **D39** (1989) 3532 and private communication.
- [14] L.V. Volkova, *Sov. J. Nucl. Phys.* **31** (1980) 784.
- [15] J. Botts, J.G Morfin, J.F. Owens, J. Qiu, W. Tung and H. Weerts, *Phys. Lett.* **B304** (1993) 159.
- [16] T.K.Gaisser: *Cosmic Rays and Particle Physics* (Cambridge University Press, 1990).
- [17] A more refined statistical treatment of the S/B discrimination will be presented by the present authors in a forthcoming paper.
- [18] D.G.Michael (MACRO Collaboration), *Nucl. Phys. (Proc. Suppl.)* **B35** (1994) 235 (Proc. TAUP 93, Ed.s C.Arpesella, E.Bellotti, A.Bottino).

Figure Captions

Figure 1 Neutralino relic abundance $\Omega_\chi h^2$ as a function of m_χ for three different neutralino compositions $P = 0.1$ (dotted line), 0.5 (short-dashed line), 0.9 (long-dashed line). The upper plot refers to positive values of μ , the lower to negative values.

Figure 2 Same as in Fig.1, except that now composition are: $P = 0.01$ (dotted line), 0.5 (short-dashed line), 0.99 (long-dashed line).

Figure 3 Scatter plot for the neutralino relic abundance $\Omega_\chi h^2$ as a function of m_χ . The two MSSM mass parameters M_2, μ are varied in the ranges: $20 \text{ GeV} \leq |\mu| \leq 3 \text{ TeV}$, $20 \text{ GeV} \leq M_2 \leq 6 \text{ TeV}$.

Figure 4 $\tanh^2(t/\tau_A)$ and Γ_A for the Earth are given as functions of m_χ , for the three representative neutralino compositions $P = 0.1$ (dotted line), 0.5 (short-dashed line), 0.9 (long-dashed line).

Figure 5 Same as in Fig.4, except that now composition are: $P = 0.01$ (dotted line), 0.5 (short-dashed line), 0.99 (long-dashed line).

Figure 6 Same as in Fig.4, except that now the neutralino local density ρ_χ is not rescaled.

Figure 7 Annihilation rate Γ_A for the Sun as a functions of m_χ , for the three representative neutralino compositions $P = 0.1$ (dotted line), 0.5 (short-dashed line), 0.9 (long-dashed line). To easily compare the annihilation rate for the Earth to the one for the Sun, the plot shown here for the Sun refers to the effective annihilation rate, defined as Γ_A times the ratio $(R_\oplus/R_\odot)^2 = 1.8 \times 10^{-9}$, where R_\oplus is the radius of the Earth and R_\odot is the Sun-Earth distance.

Figure 8 Differential neutrino spectra dN_ν/dE_ν for neutralino annihilation in the Earth, as a function of the neutrino energy E_ν . These spectra are calculated for a neutralino composition $P = 0.5$ and for three different values of neutralino mass: $m_\chi = 20 \text{ GeV}$ (dashed line), $m_\chi = 40 \text{ GeV}$ (solid line) and $m_\chi = 120 \text{ GeV}$ (dash-dotted line).

Figure 9 Flux Φ_μ of the up-going muons as functions of m_χ for χ - χ annihilation in the Earth. The threshold for the muon energy is $E_\mu^{\text{th}} = 2 \text{ GeV}$. In figure (a) the three representative neutralino compositions are $P = 0.1$ (dotted line), 0.5 (short-dashed line), 0.9 (long-dashed line). In figure (b) $P = 0.01$ (dotted line), 0.5 (short-dashed line), 0.99 (long-dashed line). The horizontal line in figure (a) represents the Kamiokande upper bound $4.0 \cdot 10^{-14} \text{ cm}^{-2} \text{ s}^{-1}$ (90 % C.L.) [2].

Figure 10 Differential muon spectra dN_μ/dE_μ as a function of the muon energy E_μ . The solid histogram is the muon spectrum obtained with our MC simulation for $P = 0.5$ and $m_\chi = 120 \text{ GeV}$. The solid line represents the muon spectrum calculated in the no-straggling approximation. The dash-dotted histogram is the muon energy distribution for the background of atmospheric neutrinos. The spectra refer to muons entering the detector within a cone of half-aperture of 30° centered at the nadir.

Figure 11 Muon angular distribution $dN_\mu/d\cos\theta$ as a function of $\cos\theta$, where θ is the nadir angle. The solid histogram is the angular distribution of the signal obtained with our MC simulation for $P = 0.5$ and $m_\chi = 120$ GeV. The dashed histogram is the muon angular distribution for the background of atmospheric neutrinos.

Figure 12 Exposure necessary to have a 4σ effect with a signal of at least 4 events, as a function of neutralino mass m_χ . The figure refers to a signal coming from the Earth. The three representative neutralino compositions are $P = 0.1$ (dotted line), 0.5 (short-dashed line), 0.9 (long-dashed line). In figure (a) At_{\min} is displayed keeping the half-aperture angle of the detector fixed at 30° from the center of the Earth. Figure (b) displays the exposure At_{opt} obtained by employing the optimization procedure.

Figure 13 Flux Φ_μ of the up-going muons as functions of m_χ for χ - χ annihilation in the Sun. The flux is orthogonal to the Sun direction and the threshold for the muon energy is $E_\mu^{\text{th}} = 2$ GeV. The three representative neutralino compositions are $P = 0.1$ (dotted line), 0.5 (short-dashed line), 0.9 (long-dashed line). The horizontal line represents the Kamiokande upper bound $6.6 \cdot 10^{-14} \text{cm}^{-2} \text{s}^{-1}$ (90 % C.L.) [2].

Figure 14 Effective exposure (ϵAt) necessary to have a 4σ effect with a signal of at least of 4 events, as a function of neutralino mass m_χ . The figure refers to a signal coming from the Sun. The three representative neutralino compositions are $P = 0.1$ (dotted line), 0.5 (short-dashed line), 0.9 (long-dashed line). The half-aperture of the detector is fixed at 5° from the Sun direction.

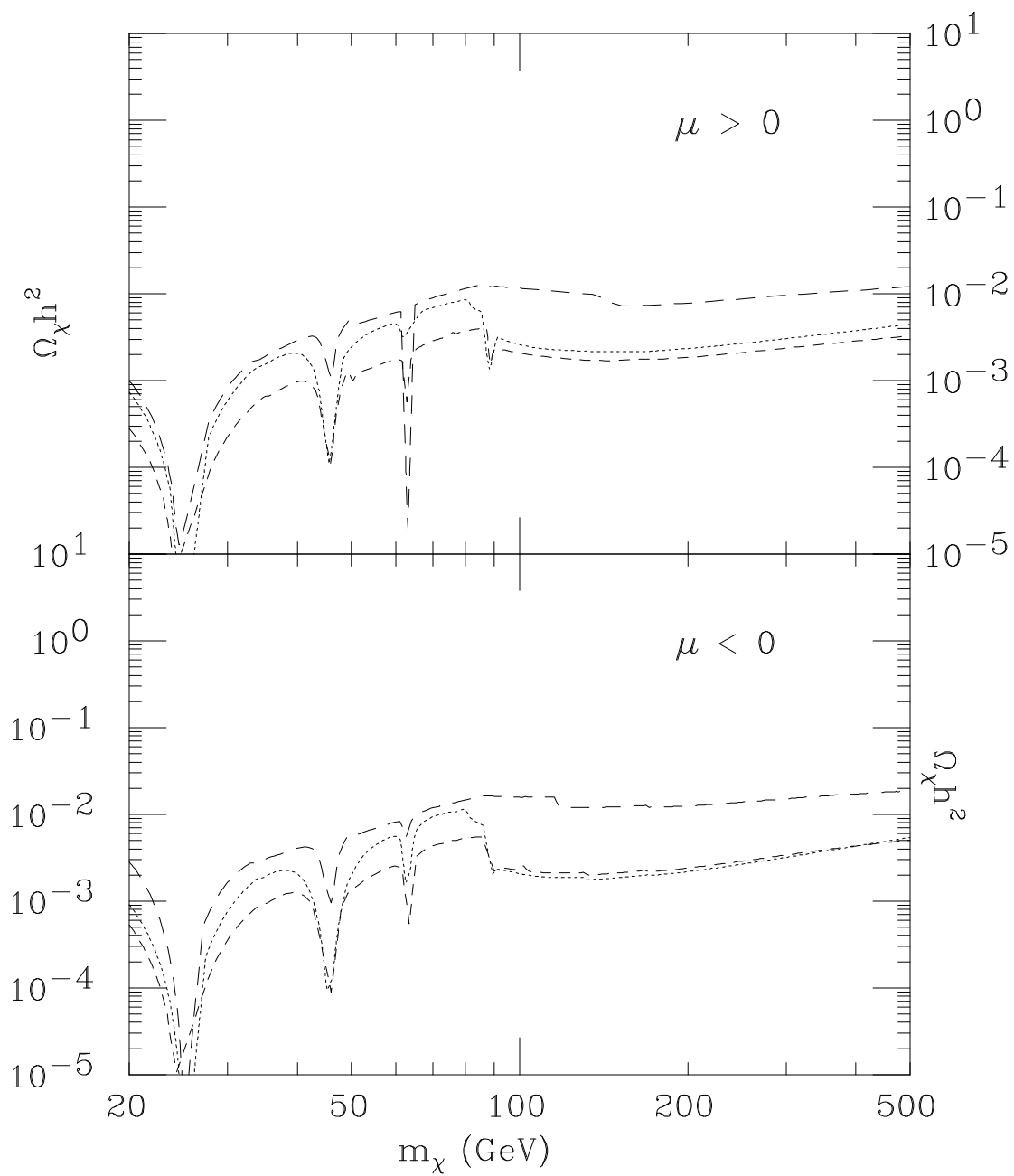


Figure 1

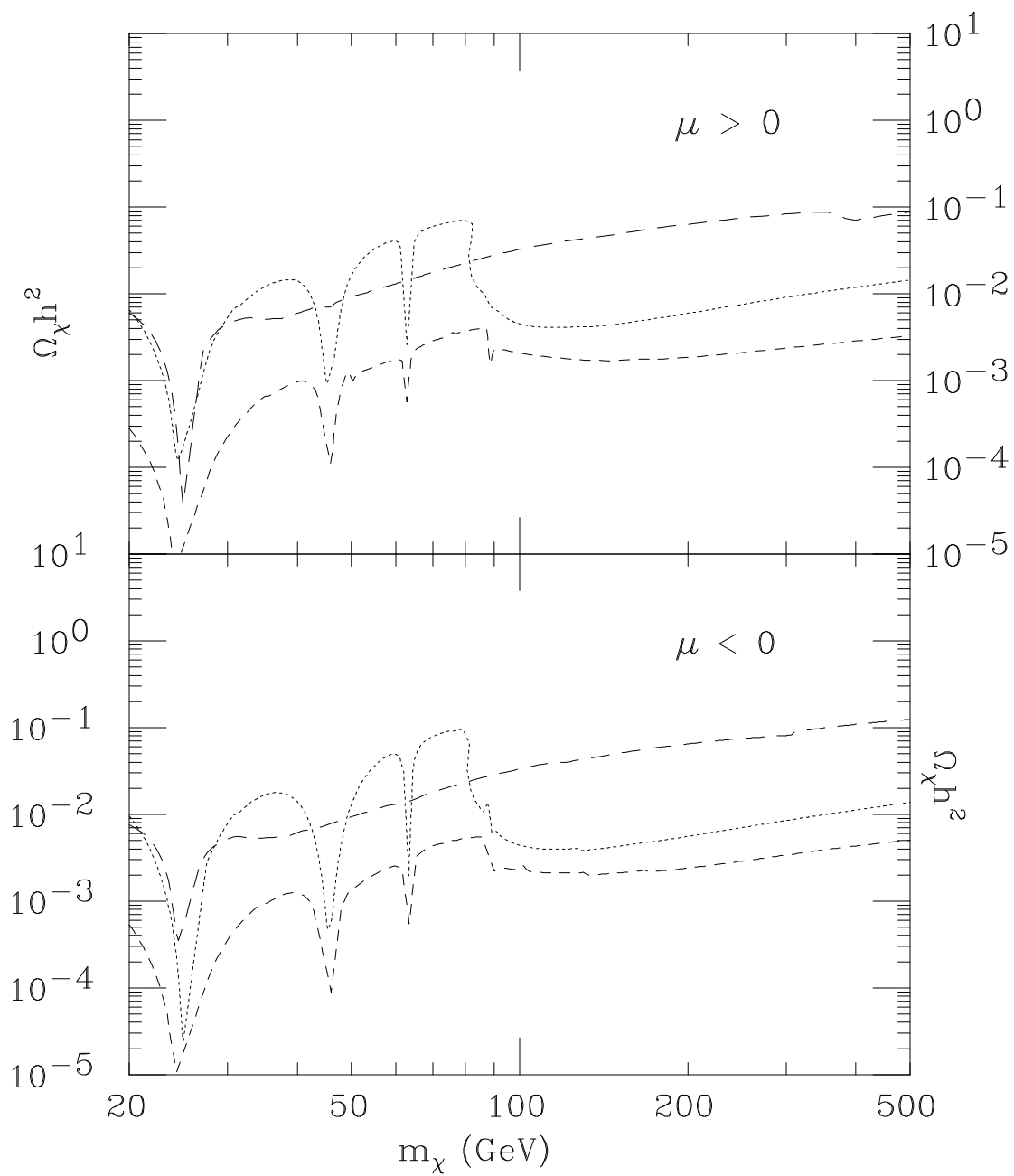


Figure 2

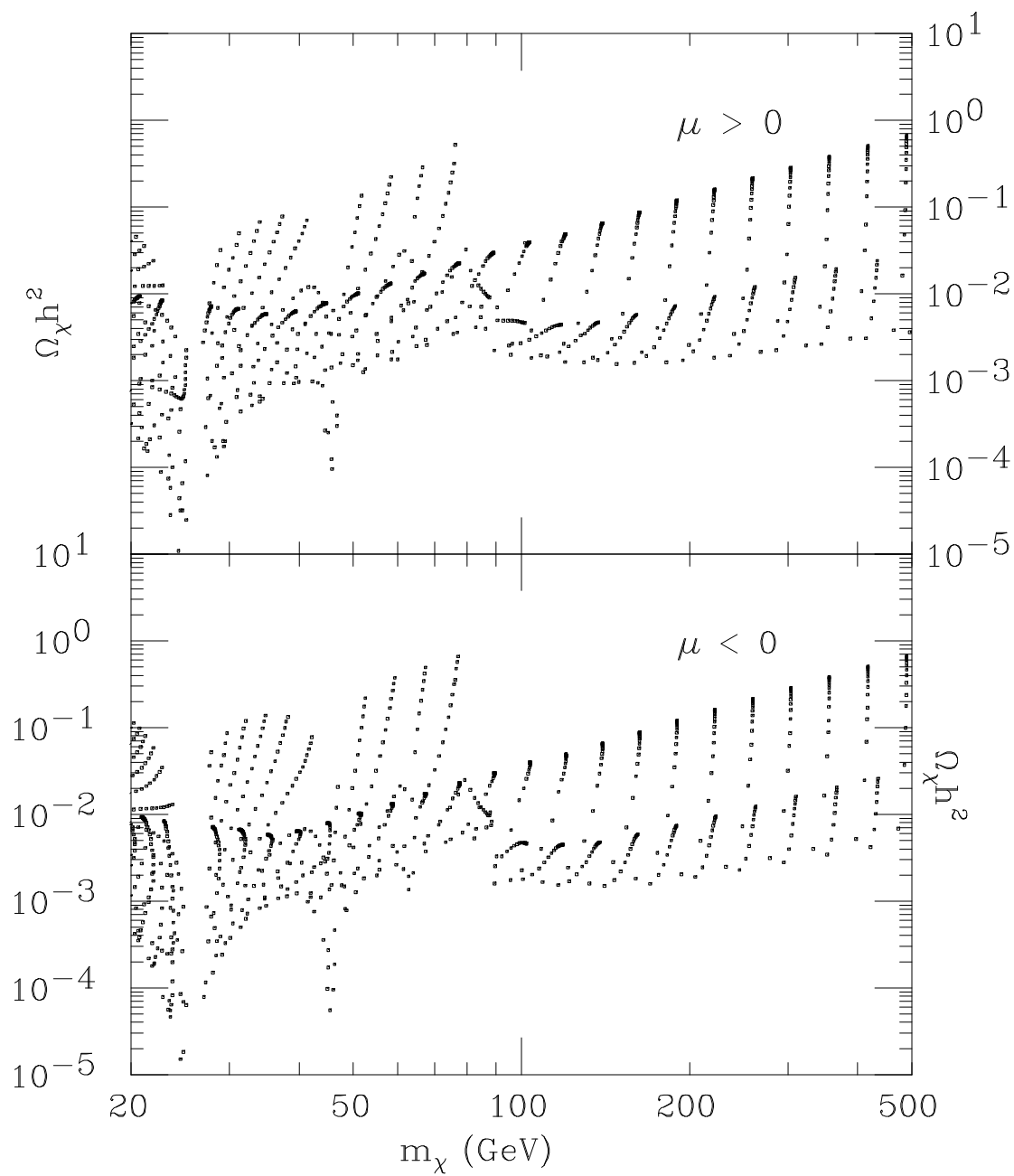


Figure 3

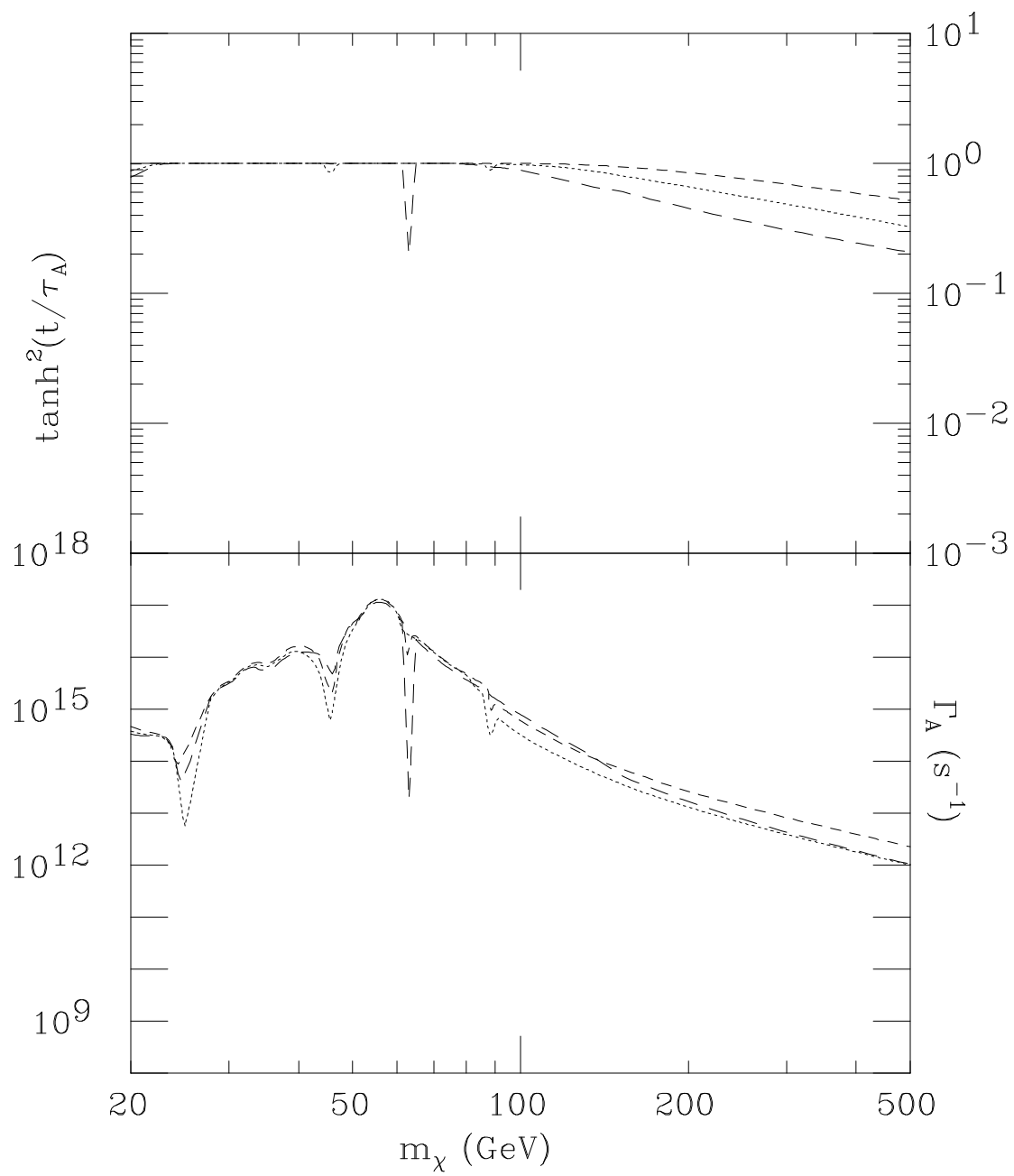


Figure 4

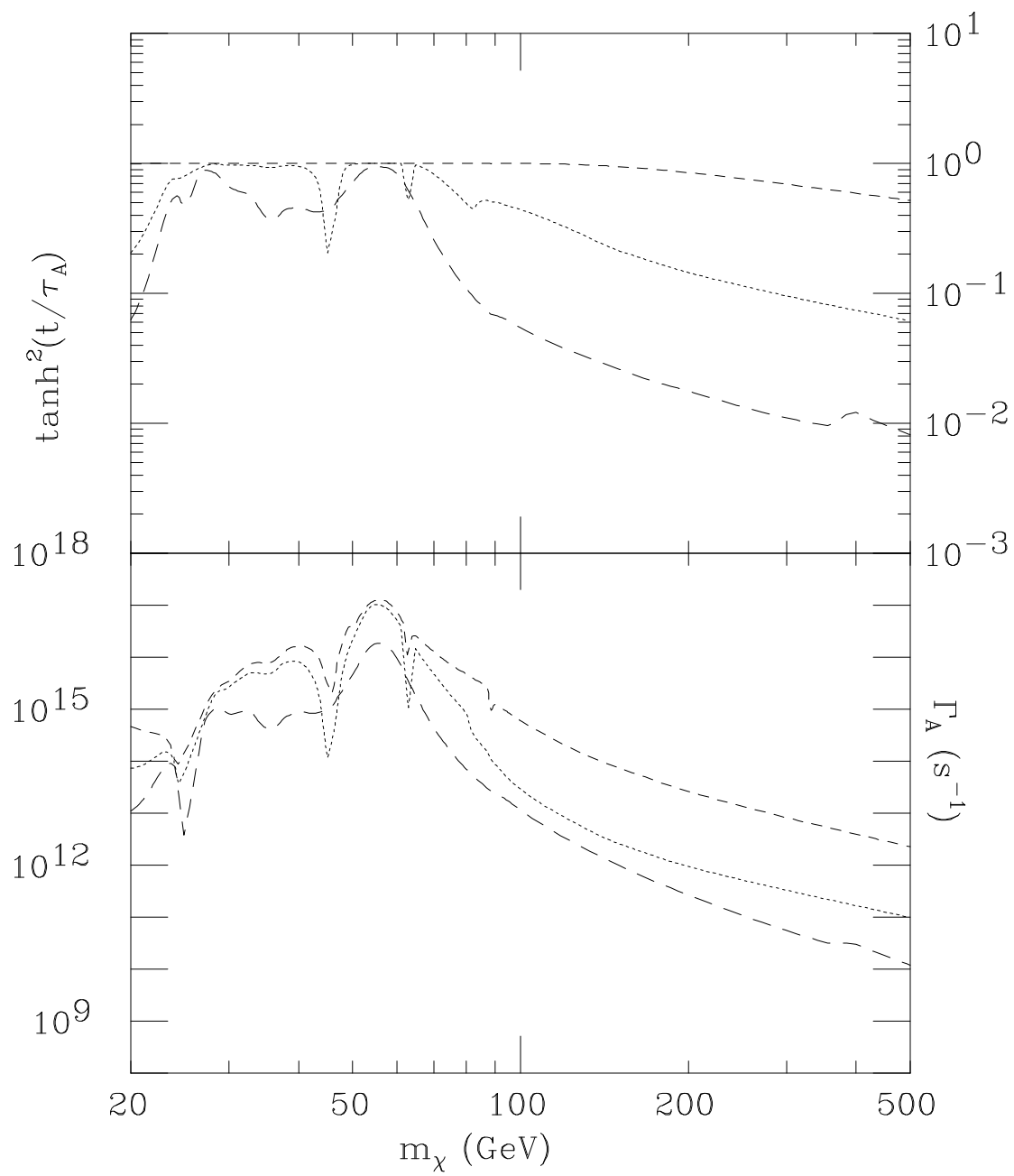


Figure 5

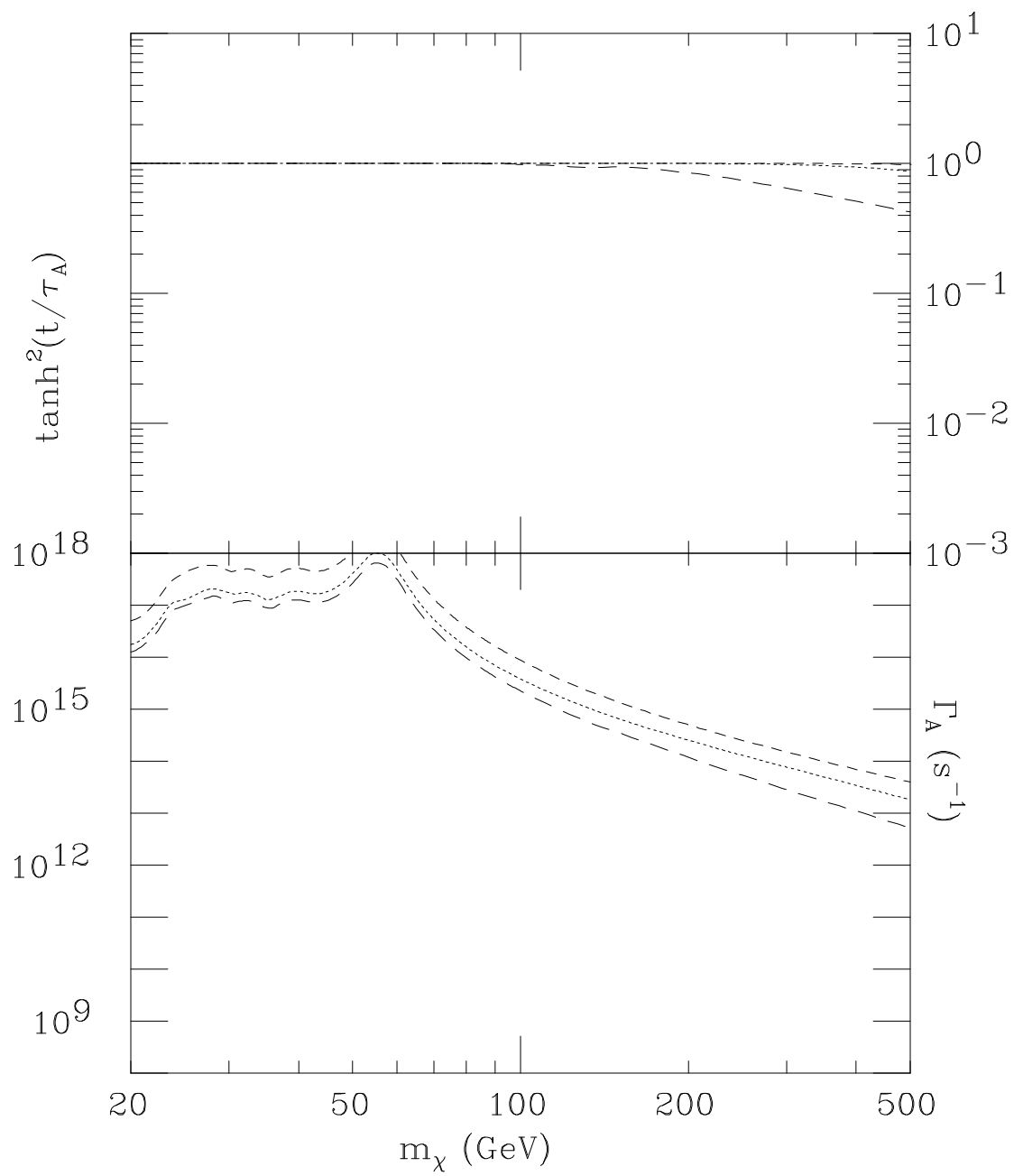


Figure 6

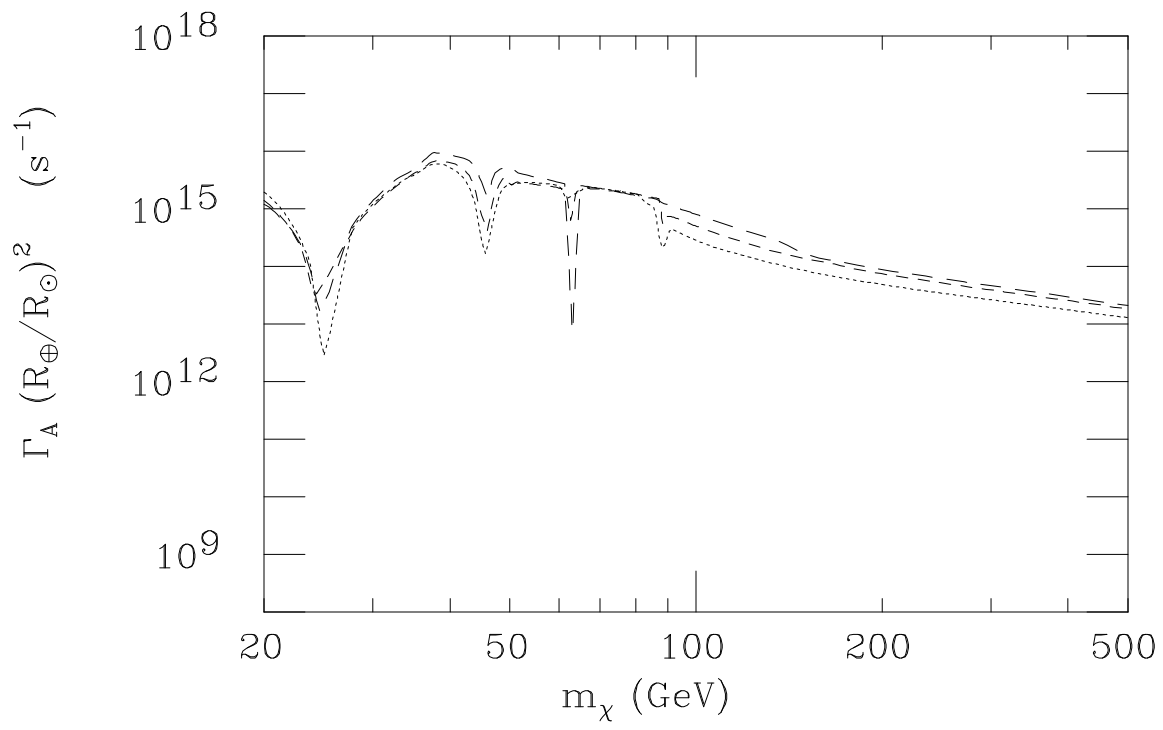


Figure 7

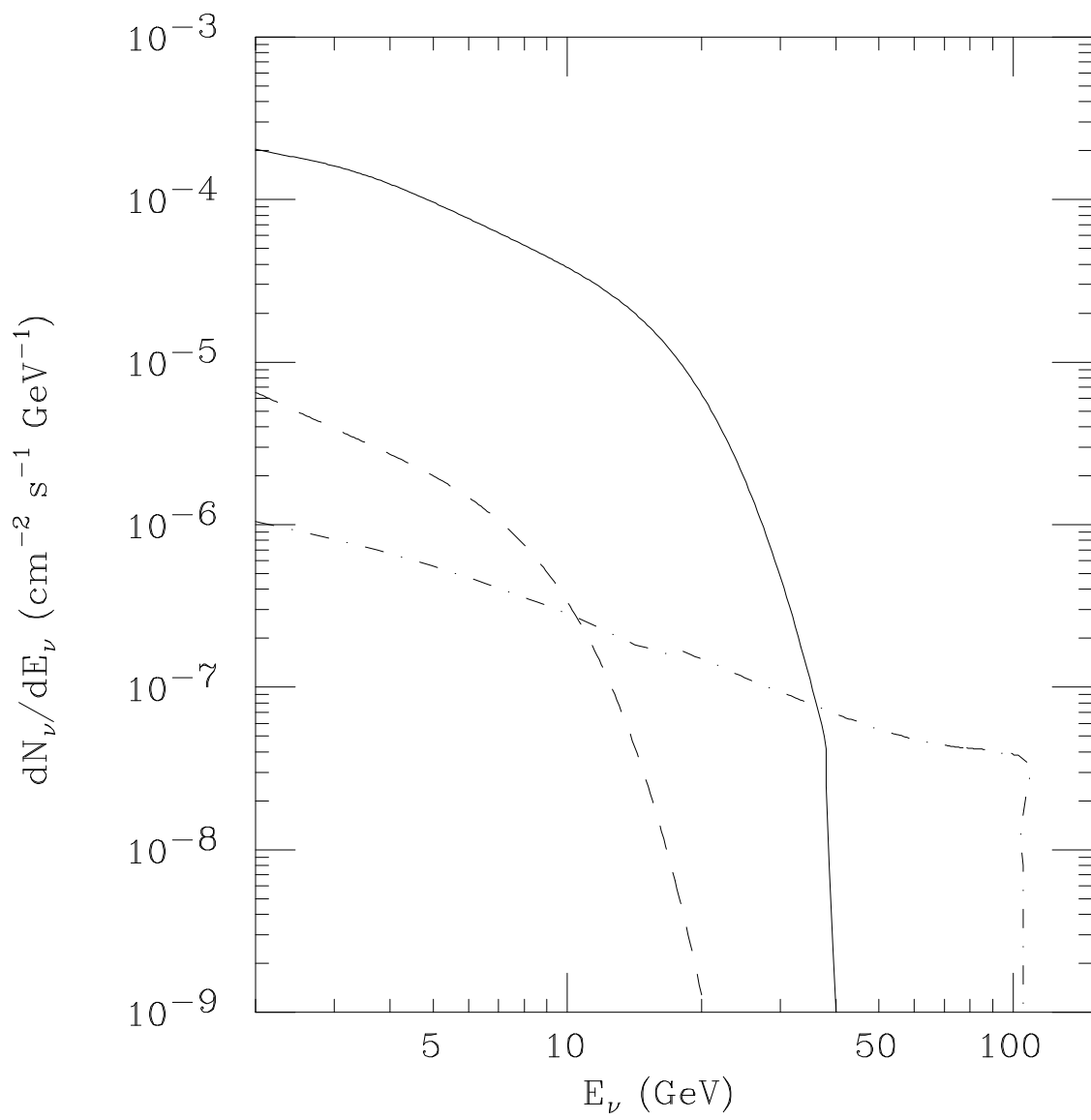


Figure 8

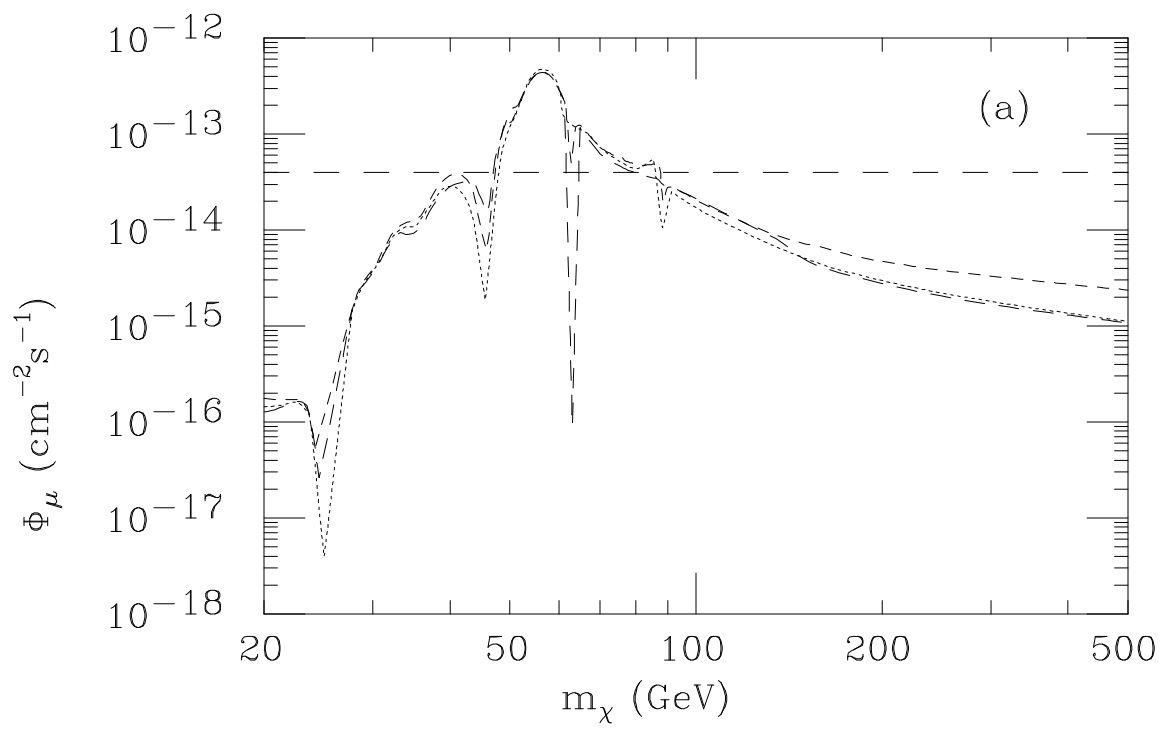


Figure 9a

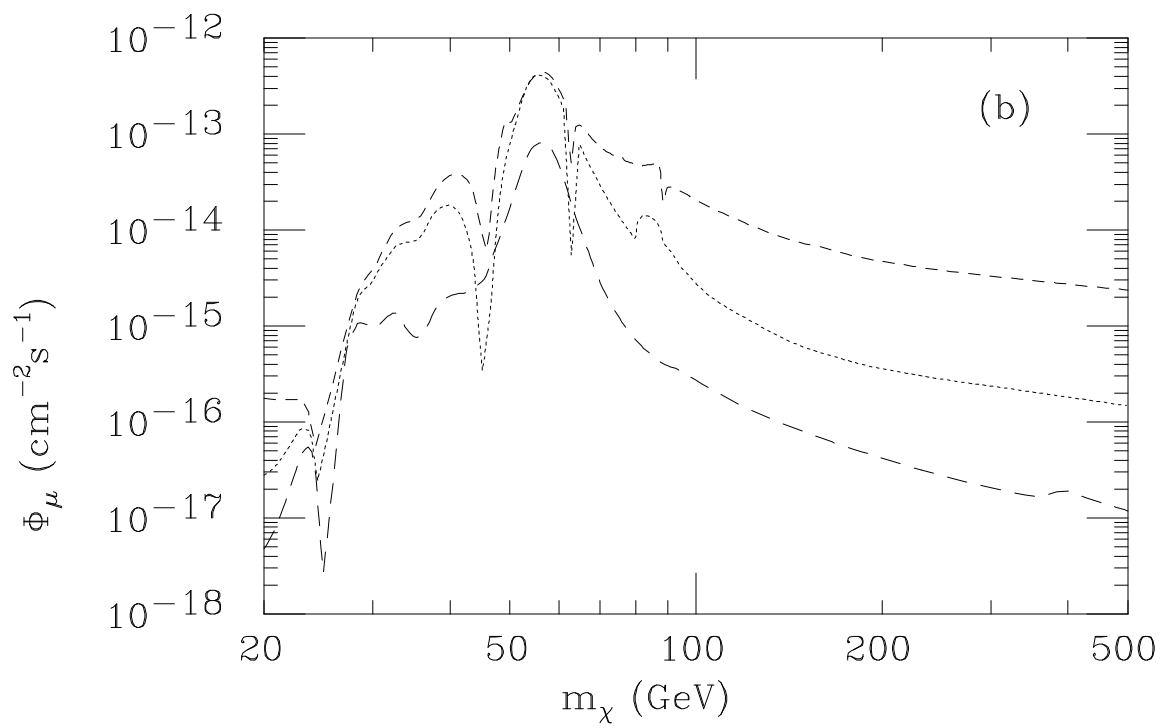


Figure 9b

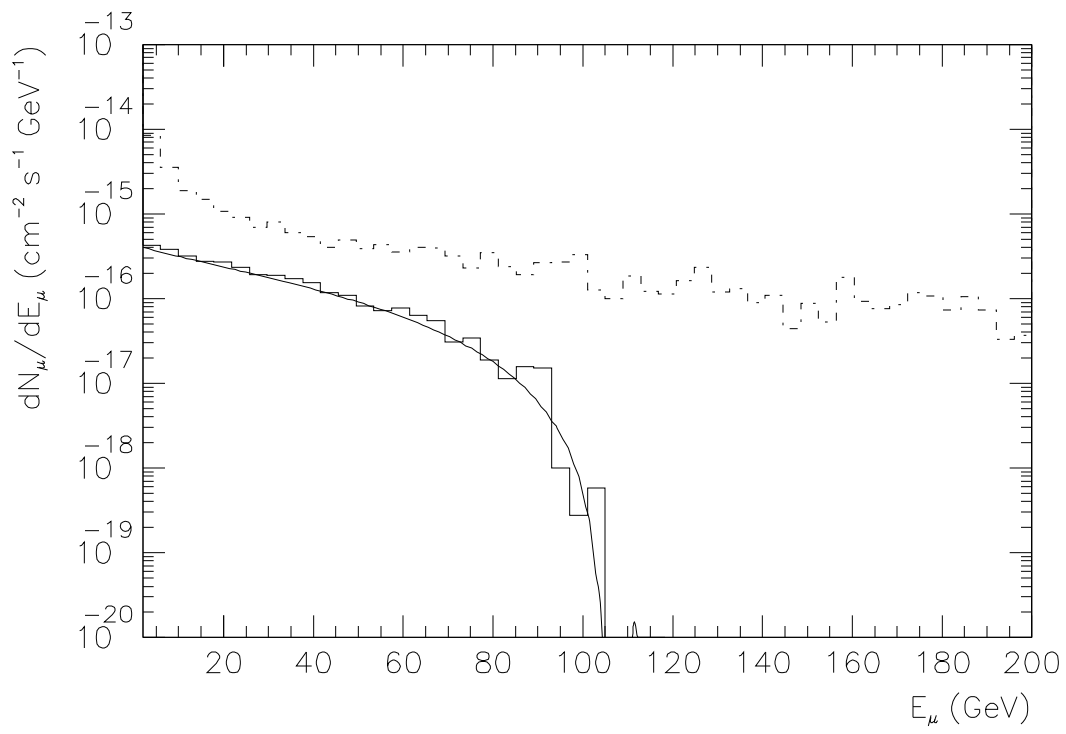


Figure 10

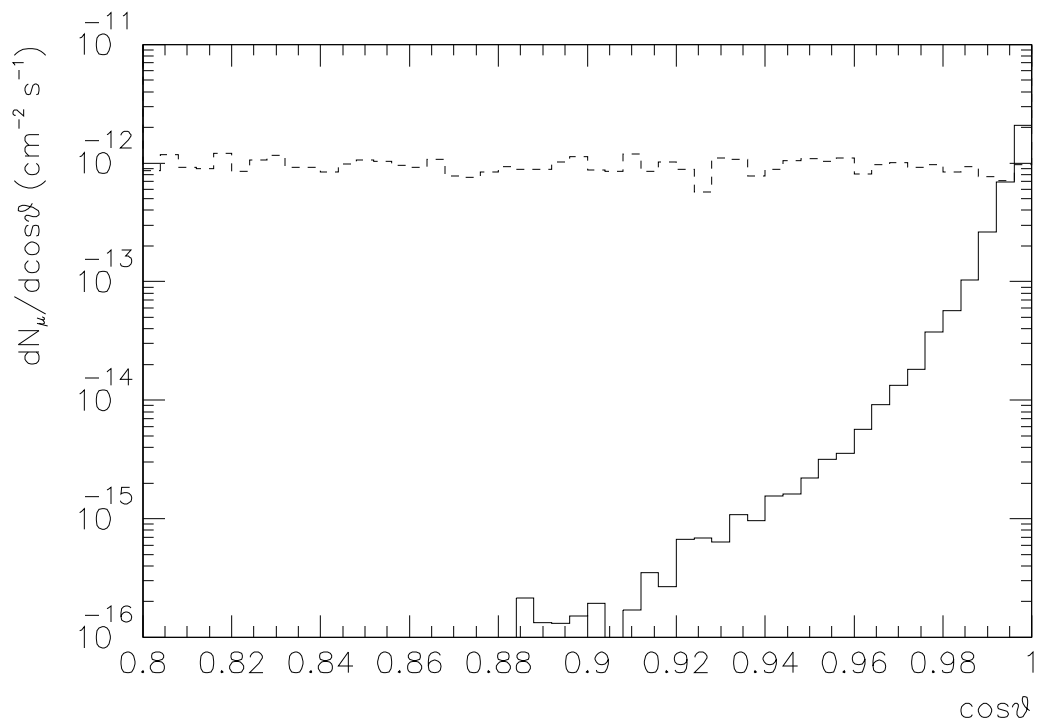


Figure 11

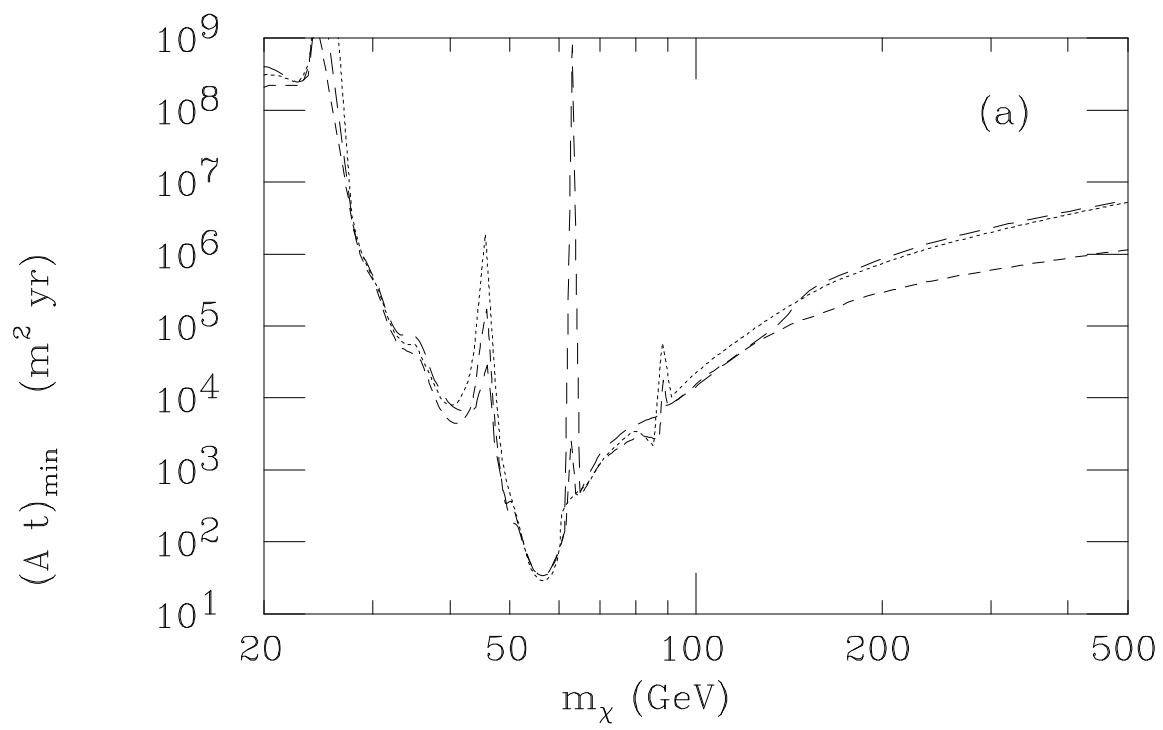


Figure 12a

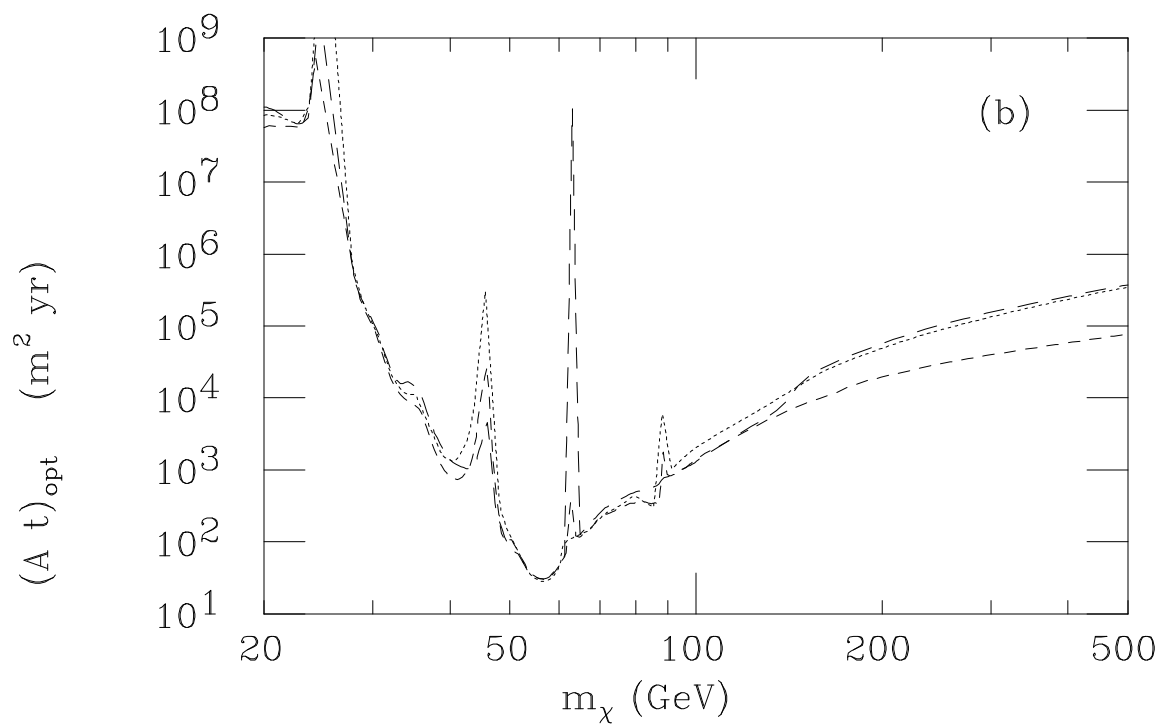


Figure 12b

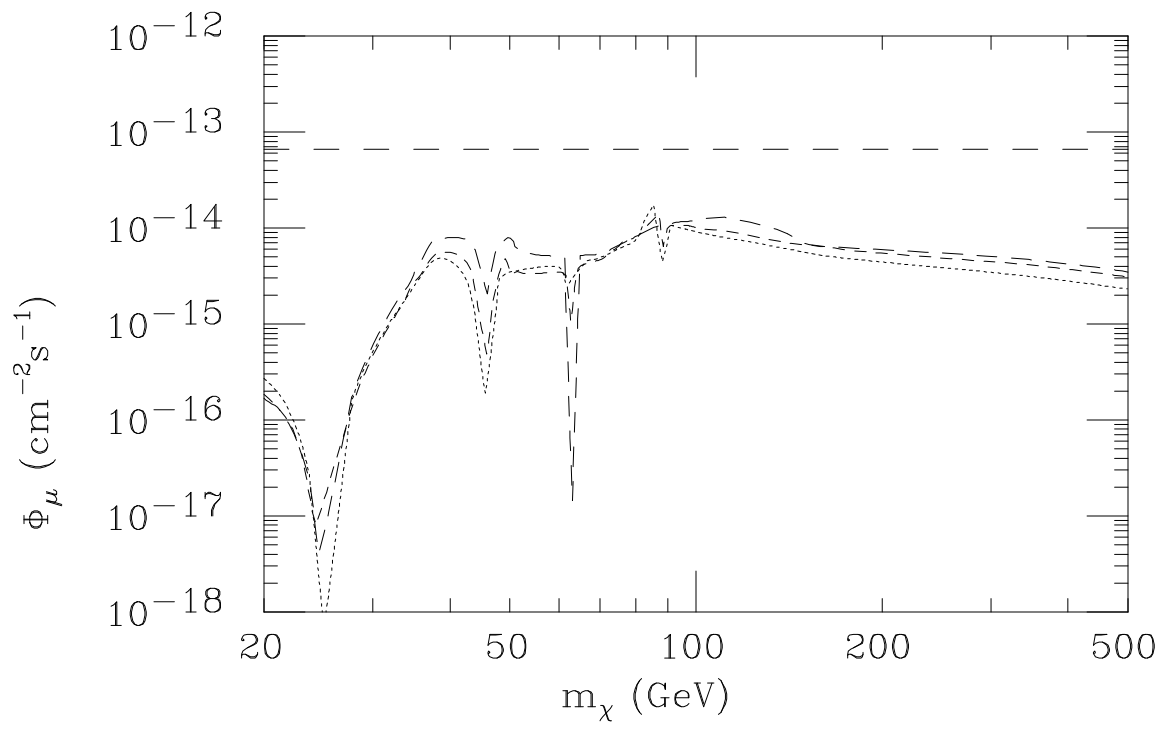


Figure 13

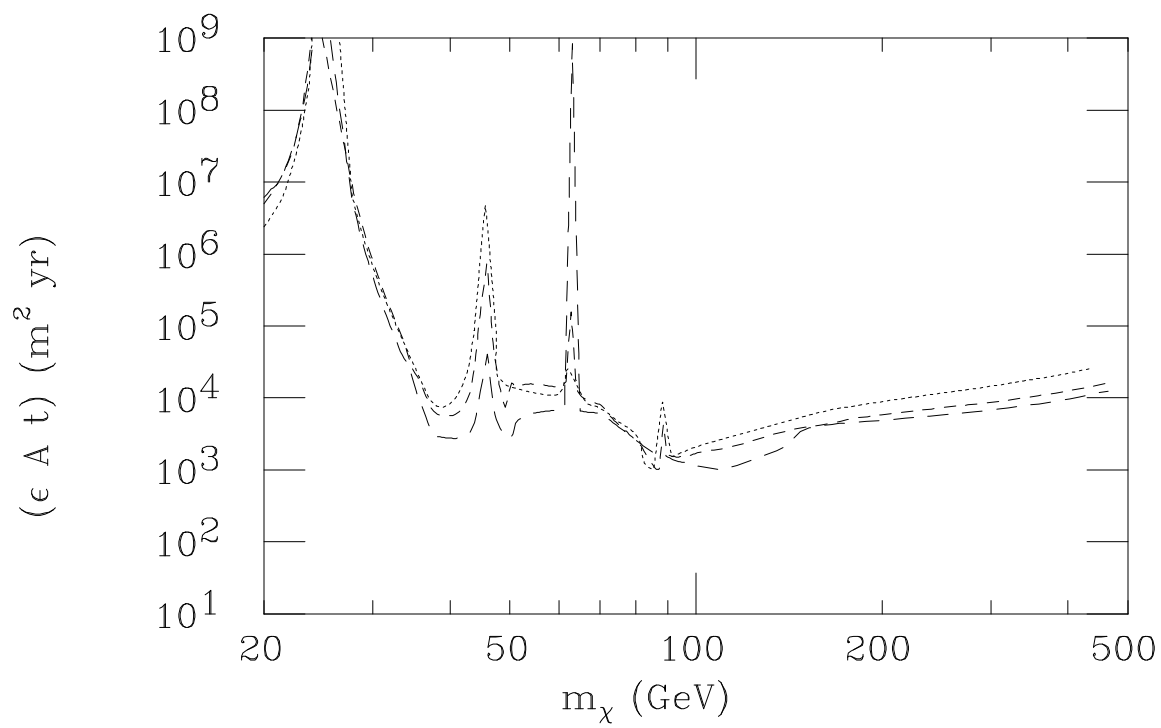


Figure 14